An Analytical Framework for Determining the Minimum Size of Highly Miniaturized Satellites: PlanarSats

Uludag, M.S.; Aslan, Alim Rüstem

DOI
10.3390/aerospace12100876

Publication date
2025

Document Version
Final published version

Published in
Aerospace

aerospace

MDPI

Article

An Analytical Framework for Determining the Minimum Size of Highly Miniaturized Satellites: PlanarSats

Mehmet Şevket Uludağ [1,2,*] and Alim Rüstem Aslan [2]

[1] Faculty of Aerospace Engineering, Delft University of Technology, Kluyverweg 1, 2629 HS Delft, The Netherlands
[2] Faculty of Aeronautics and Astronautics, Istanbul Technical University, Ayazağa Campus, Istanbul 34469, Turkey; aslanr@itu.edu.tr
* Correspondence: m.s.uludag@tudelft.nl

Abstract

This paper introduces a power-driven systems engineering methodology for the early-phase design of highly miniaturized satellites: PlanarSats. We derive an analytical framework linking power requirements, contingency policies, solar-cell performance, and subsystem integration to determine the absolute minimum satellite size. Through idealized and detailed case studies, we explore the trade-offs inherent in subsystem selection and integration constraints. Sensitivity analysis identifies critical factors affecting minimum area and operational envelopes. Our framework provides a clear tool for balancing functionality, reliability, and physical limits in next-generation ultra-small satellite missions.

Keywords: PlanarSat; attosat; femtosat; ChipSat; small satellite; systems engineering

check for updates

Academic Editors: Ed Kruzins and Edwin Peters

Received: 30 June 2025
Revised: 10 September 2025
Accepted: 17 September 2025
Published: 28 September 2025

Citation: Uludağ, M.Ş.; Aslan, A.R. An Analytical Framework for Determining the Minimum Size of Highly Miniaturized Satellites: PlanarSats. *Aerospace* **2025**, *12*, 876. https://doi.org/10.3390/aerospace12100876

1. Introduction

The relentless miniaturization of space systems has given rise to a new class of highly integrated, highly miniaturized spacecraft: femtosatellites and attosatellite platforms, including PlanarSats. These spacecraft push the boundaries of what is physically and technologically feasible in orbit, enabling new opportunities for distributed sensing, rapid technology demonstration, and cost-effective access to space [1]. However, as system size shrinks, designers face severe constraints: limited surface area for power generation, difficulties in integrating all essential subsystems (such as communications, attitude control, and payload), and maintaining a basic level of operational capability.

In this work, a "PlanarSat" refers to a quasi-two-dimensional, highly miniaturized spacecraft comprising a single thin substrate as the main structure, with solar cells and electronic components mounted on one or both faces. Depth available for stacking is negligible; functions are realized as planar blocks on the two surfaces. The minimum feasible size is therefore governed jointly by the area needed to generate power and the area needed to place electronics.

While standards like CubeSat [2] and PocketQube [3] have advanced small satellite engineering, current design methodologies do not address the unique constraints of the atto- and femto-class. In this size regime, surface area, power budget, and subsystem integration are tightly coupled, and traditional mass- or volume-based scaling relations are not sufficient. Most prior studies focus on larger satellites, partly due to the limited number of missions at the femto- and attosatellite scale [4,5]. These prior works primarily provide surveys and technology overviews rather than analytical methods, leaving a distinct analytical gap regarding the true minimum size of a satellite that can function reliably

in orbit, dictated primarily by power generation and physical integration limits. Although some studies explicitly explore extremely small-scale satellites, such as Barnhart et al.'s PCBSat [6,7], comprehensive analytical treatments defining fundamental size constraints for atto- and femto-scale spacecraft remain limited. A complementary study on Smart-Dust femtosatellites reviews propellantless, SRP-driven devices with a very high area-to-mass ratio, covering architecture, attitude/control approaches, and orbit-dynamics-driven mission concepts [8]. Our work differs in that we develop a power-driven minimum-size framework for planar, two-sided satellites where the surface area must simultaneously host solar cells and electronics.

A fundamental and still unsolved question is the following: What sets the minimum feasible size for a highly miniaturized satellite? Unlike larger spacecraft, where mass and volume constraints can often be overcome with advances in materials or manufacturing, ultra-small platforms encounter unavoidable geometric limits. Below a certain area, it is simply impossible to generate enough power, house the required electronics, or operate basic satellite functions, regardless of improvements in technology or packaging. In atto- and femto-scale platforms, this interplay of mission requirements, technology, and fundamental physics imposes a lower bound on system size. Other potential constraints, such as thermal management, radiation tolerance, and launch survivability, may also become critical; however, they are beyond the scope of this study and are left for future research.

This work directly addresses this gap by presenting an analytical framework for estimating the minimum feasible size of a PlanarSat, based on the interdependency of power demand, design contingency, solar-cell efficiency, and electronics integration. By relating practical design requirements to physical parameters, such as the solar-cell fill ratio and subsystem surface area, we provide a transparent method for computing a lower-bound area needed for reliable operation.

Our approach enables rapid, early-phase feasibility assessment for novel satellite concepts and provides a clear foundation for future advances in highly miniaturized satellite architectures. The results offer a tool for system-level trade studies and mission planning, establishing an analytically motivated lower-bound estimate on the size of atto- and femto-scale spacecraft within the stated scope of power generation and planar integration limits.

We address power and area first because continuous power generation is a necessary condition for any active function at these scales; without it, other subsystem trades become moot. Moreover, the surface area, shared between cells and electronics, often becomes the tightest physical constraint. Accordingly, we focus on power generation and planar integration as the first-order limiter, and we explicitly note that detailed mass, thermal, electromagnetic compatibility, and link-budget analyses are outside this paper's scope and are left for future work.

This paper makes four focused contributions for early-phase PlanarSat design. (i) It formalizes a stepwise sizing method that maps peak mode power (CBE), a design contingency C, and technology parameters to the active and physical solar-cell areas, and then to the installed satellite area for a separated baseline, keeping power-path losses counted once in the mode sums. (ii) It derives architecture-dependent allocation expressions for separated, half-mixed, and mixed layouts, clarifying that instantaneous electrical power is produced by the sunlit face only and that "mixed, per-face sufficiency" trades extra installed area for robustness to which face is illuminated. (iii) It defines an operational envelope from a cosine incidence model, relating continuous-operation angles directly to the ratio of mode demand to contingency-corrected capacity. (iv) It quantifies the sensitivity of the required area to solar-cell efficiency, power-path efficiency, and fill ratio, and it illustrates

the framework on a realistic part set with a conservative packaging factor for peripherals and routing.

In early-phase studies, a defensible lower bound on an installed surface area is not a cosmetic metric; it gates feasibility. First, it provides a go/no-go screen for a given payload–COMM concept: if the contingency-corrected peak load cannot be met by the power that fits on the available faces, the concept is infeasible independent of later subsystem refinements. Second, it selects between layouts: when $A_{\text{cell,phys}} > A_{\text{electronics,tot}}$, a separated layout minimizes the installed area. Missions that cannot guarantee which face is sunlit benefit from mixed layouts that trade extra area for per-face sufficiency (Section 4.1). Third, it directs technology effort and procurement: the sensitivity in Section 6 quantifies which levers ($\eta_{\text{cell}}, \eta_{\text{power}}, \eta_{\text{infill}}$) most effectively reduce the required *cell* area; packaging-factor effects enter analytically through Equation (1) as $A_{\text{electronics,tot}} = \sum_j \kappa_{\text{pack},j} A_{\text{IC},j}$ and then translate to the installed area via Equations (8), (10) and (11).

Operationally, the minimum area links directly to usable Sun off-pointing: with arrays sized at normal incidence to meet MEV, the continuous-operation angle is $\theta_{\max} = \arccos(\text{CBE}/\text{MEV})$, so shortfalls in the installed area collapse the geometric envelope in Section 5. In practice, this early bound also informs external interfaces (deployer aperture, keep-outs) and attitude expectations in LEO, where the choice of which face is illuminated cannot be guaranteed without control and, hence, neither can the value of per-face sufficiency. These points clarify why establishing the minimum size early is a substantive design decision rather than an aesthetic preference.

2. Parameters Used to Design a PlanarSat

To outline an effective approach to PlanarSat design, it is essential to first clarify the parameters and constraints involved. The following definitions lay the groundwork for the analytical framework used throughout this work, showing how the minimum installed area follows from power and placement considerations. Key variables used in this paper are summaried in Table 1.

The current best estimate (CBE) denotes the peak instantaneous electrical power required across operational modes (sum of active functions in that mode). A design contingency C is applied to the CBE to obtain the maximum expected value (MEV); the MEV is the target power that the solar array must be capable of providing at the sizing point. The electrically active solar area required is set by the power target and by technology/geometry factors (AM0 irradiance and cell efficiency), while the physical installed area is set jointly by this active area (through the fill ratio) and by the electronics placement area.

Table 1. Summary of key variables used in the framework.

Symbol	Description	Units
CBE	Current Best Estimate (peak mode power demand)	mW
MEV	Maximum Expected Value (power with contingency)	mW
$I_{Solar,E}$	AM0 solar irradiance at Earth orbit	mW/cm^2
η_{cell}	Solar-cell efficiency (electrical out/solar in)	–
η_{power}	Power-path efficiency (MPPT × regulator)	–
η_{infill}	Solar-cell fill ratio (active area fraction)	–
A_{IC}	Bare IC/package footprint area	cm^2
κ_{pack}	Electronics layout factor (area multiplier per IC)	–
$A_{\text{electronics,tot}}$	Total electronics area (incl. A_{IC}/passives/routing)	cm^2
$A_{\text{cell,tot}}$	Active solar-cell area (electrically producing)	cm^2
$A_{\text{cell,phys}}$	Physical cell area ($A_{\text{cell,tot}}/\eta_{\text{infill}}$)	cm^2
$A_{\text{satellite}}$	Total installed satellite surface area (sizing result)	cm^2

Unless stated otherwise, η_{power} and κ_{pack} are treated as parameters, not fixed constants. The total electronics placement area follows the bookkeeping relation

$$A_{\text{electronics,tot}} = \sum_j \kappa_{\text{pack},j}\, A_{\text{IC},j}. \tag{1}$$

In this work, we adopt a planar spacecraft form factor ("PlanarSat"), in which a single thin substrate serves as the primary structure and functional elements are realized as blocks on one or both faces. Because out-of-plane stacking is negligible, the minimum size is governed jointly by (i) the area needed to generate continuous power and (ii) the area needed to place electronics.

To illustrate the coupling between "power cost" and "placement cost" at the part level, consider the STM32L496RGT6 microcontroller [9], with footprint $A_{\text{IC}} \approx 1.96$ cm^2 and peak supply ≈ 42 mW. Using representative space-qualified cells (e.g., Azur Space 3G30A [10]) at AM0 $I_{Solar,E} \approx 136.1$ mW/cm^2 and $\eta_{\text{cell}} \approx 0.30$, the available panel density is ≈ 40.8 mW/cm^2, so the active cell area needed solely for the MCU at peak load is

$$A_{\text{cell,tot,MCU}} \approx \frac{42\ \text{mW}}{136.1\ \text{mW/cm}^2 \times 0.30} \approx 1.03\ \text{cm}^2, \tag{2}$$

ignoring conversion losses for this illustrative part-level estimate. The corresponding physical installed area is $A_{\text{cell,phys,MCU}} = A_{\text{cell,tot,MCU}}/\eta_{\text{infill}}$. Figure 1 visualizes this part-level surface budget: the black box is the integrated circuit (IC) footprint A_{IC}, the blue label indicates electrical load, and the blue-shaded bars show the active and physical solar-cell area required to supply that load at AM0 with $\eta_{\text{cell}} = 30\%$ and fill ratio η_{infill}. The plot emphasizes that even modest peak loads impose a non-negligible cell-area penalty at this scale.

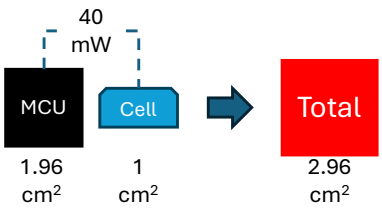

Figure 1. Surface cost of an IC: its footprint, required power, and the solar-cell area needed to generate that power. Example assumes that the AM0 $I_{Solar,E} = 136.1$ mW/cm^2 and $\eta_{\text{cell}} = 30\%$; thus, ≈ 40.8 mW/cm^2 is available.

Each functional group (e.g., microcontroller (MCU), transceiver, payload) is thus associated with a placement cost (A_{IC} scaled by κ_{pack}) and a power cost ($A_{\text{cell,tot}}$ scaled by η_{infill} to obtain $A_{\text{cell,phys}}$). The minimum installed area $A_{\text{satellite}}$ must satisfy both the placement and power simultaneously; subsequent sections formalize this with sizing expressions and architecture-dependent layouts.

3. Idealized Model

3.1. Minimum Recommended Satellite Area

When starting a PlanarSat project, it is essential to establish the key variables that set the recommended minimum installed area. In this size regime, the surface area, power budget, and subsystem integration are tightly coupled; the sizing links contingency-corrected power to the active solar area and to the physical area needed on the panels.

Selecting an appropriate contingency is central to realistic sizing because it accounts for uncertainties at different design phases and mission classes. Table 2 [11] summarizes the recommended reserves adapted and extended from AIAA guidelines [12] with class

definitions following [13]. Program phases typically progress through Bid, conceptual design review (CoDR), Preliminary design review (PDR), Critical design review (CDR), and flight readiness review (FRR); contingency generally decreases as design maturity increases [11].

Power-Driven Sizing Sequence

Let CBE denote the peak instantaneous mode power. Apply contingency C to obtain the MEV, and then map power to area:

1. **Peak mode power (CBE).**

$$\mathrm{CBE} = \max_{\mathrm{mode}} \sum_{i} P_{\mathrm{function},i} \tag{3}$$

2. **Contingency application.**

$$\mathrm{MEV} = (1 + C)\,\mathrm{CBE}. \tag{4}$$

3. **Active solar area at the sizing point.**

$$A_{\mathrm{cell,tot}} = \frac{\mathrm{MEV}}{I_{\mathrm{Solar,E}}\,\eta_{\mathrm{cell}}}. \tag{5}$$

4. **Optional orbit/incidence derating.** Define $\gamma_{\mathrm{orbit}} \in (0, 1]$ as the product of the expected sunlit duty cycle and the cosine-averaged projected area for the target orbit and attitude statistics. If a team prefers to include this effect in sizing rather than in the envelope analysis of Section 5, Equation (5) becomes

$$A_{\mathrm{cell,tot}} = \frac{\mathrm{MEV}}{I_{\mathrm{Solar,E}}\,\eta_{\mathrm{cell}}\,\gamma_{\mathrm{orbit}}}. \tag{6}$$

   In the results reported here, we set $\gamma_{\mathrm{orbit}} = 1$ and treat off-normal incidence and eclipse explicitly in Section 5 (geometric envelope and orbit propagation from a published TLE). Teams who prefer to fold orbit statistics directly into sizing may choose $\gamma_{\mathrm{orbit}} < 1$; in that case, the envelope in Section 5 should be interpreted as a geometric check rather than an additional derating to avoid double counting. As a simple illustration, a sunlit-duty factor of 0.62 and an average $\langle \cos\theta \rangle$ of 0.85 gives $\gamma_{\mathrm{orbit}} \approx 0.53$, increasing the required active area by a factor of $1/0.53 \approx 1.9$ at the same MEV.

   Here, η_{cell} may be taken at BOL or EOL (including temperature and spectral derating where available); using an EOL dataset directly substitutes that value in Equation (5).

5. **Physical installed cell area.**

$$A_{\mathrm{cell,phys}} = \frac{A_{\mathrm{cell,tot}}}{\eta_{\mathrm{infill}}}. \tag{7}$$

6. **Installed satellite area for the separated baseline.**

$$A_{\mathrm{satellite}} = \max\left(A_{\mathrm{cell,phys}},\, A_{\mathrm{electronics,tot}}\right). \tag{8}$$

In this work, η_{cell} denotes an effective solar-cell efficiency at the selected operating point. If an end-of-life dataset is preferred, that value is used directly in Equation (5) in place of a nominal one, and no additional factors are introduced. Mode sums used to compute CBE already include maximum power point tracking (MPPT) and regulation losses; therefore, Equations (5)–(7) are not divided by a separate power-path efficiency in

order to avoid double counting. The translation from $A_{\text{cell,phys}}$ and $A_{\text{electronics,tot}}$ to the final installed area, $A_{\text{satellite}}$, depends on the surface layout; alternate architectures modify only the allocation step via the expressions in Section 4.1. Here, $A_{\text{electronics,tot}}$ is computed from the part footprints via the packaging factor κ_{pack} (see Equation (1) and Table 1).

Table 2. Extended recommended power contingencies based on AIAA minimum standard reserves [12]. Original anchors are retained; *italicized entries are extrapolated for refined low-power bins*. "Bid" is the proposal phase; CoDR is Concept Design Review; PDR is Preliminary Design Review; CDR is Critical Design Review; PRR/FRR is Production or Flight Readiness Review. Class definitions follow [13].

	Proposal Stage			**Design Development Stage**									
	Bid Class			**CoDR Class**			**PDR Class**			**CDR Class**			**PRR/FRR Class**
Description/ Categories	**I**	**II**	**III**	**I**	**II**	**III**	**I**	**II**	**III**	**I**	**II**	**III**	**I-II-III**
0–1.2 W	*120*	*65*	*13*	*105*	*50*	*12*	*70*	*45*	*9*	*45*	*40*	*7*	*5*
1.2–5 W	*115*	*60*	*13*	*100*	*45*	*12*	*65*	*40*	*9*	*40*	*35*	*7*	*5*
5–20 W	*110*	*55*	*13*	*95*	*40*	*12*	*60*	*35*	*9*	*35*	*30*	*7*	*5*
20–50 W	*105*	*50*	*13*	*90*	*35*	*12*	*55*	*30*	*9*	*30*	*25*	*7*	*5*
50–100 W	*100*	*45*	*13*	*85*	*30*	*12*	*50*	*25*	*9*	*25*	*20*	*7*	*5*
100–500 W	90	40	13	75	25	12	45	20	9	20	15	7	5
500–1500 W	80	35	13	65	22	12	40	15	9	15	10	7	5
1500–5000 W	70	30	13	60	20	12	30	15	9	15	10	7	5
5000 W+	40	25	13	35	20	11	20	15	9	10	*7*	7	5

3.2. Power Requirement Estimation of a PlanarSat

This section establishes the baseline power requirement (CBE) from a minimal, three-function PlanarSat: an MCU (serving as on-board computer (OBC)), a payload, and a single transceiver IC. These supply powers are taken directly from part datasheets for a representative configuration; conversion losses and additional RF stages (e.g., PA, LNA) are not included here but are addressed later in the detailed example (Section 4.3).

Baseline Parts and Footprints

We use commercially available components: STM32L496RGT6 (MCU, 1.96 cm^2, 30 mW at 16 MHz) [9], SX1278IMLTRT (sub-GHz transceiver, 0.49 cm^2, 95.7 mW in TX at 13 dBm, 40 mW in RX) [14], and a representative payload (2.00 cm^2, 50 mW). These values are provided as a placeholder to demonstrate the sizing flow on a minimal part set (e.g., a simple sensor plus conditioning); the framework is configurable for various payloads, enabling use of mission-specific components with different power and size requirements. The baseline components and their footprints/powers are summarized in Figure 2.

The "generic payload" above is a proxy for low-rate sensing with simple conditioning; it serves only to demonstrate the sizing flow. For any payload with footprint A_{payload} and supply power P_{payload}, the mode sums and placement bookkeeping become

$$\begin{aligned} P_{\text{Payload mode}}(P_{\text{payload}}) &= 30 + 40 + P_{\text{payload}} \quad \text{(mW)}, \\ P_{\text{TX mode}} &= 30 + 95.7 \quad \text{(mW)}, \\ \text{CBE} &= \max\left(P_{\text{Payload mode}}(P_{\text{payload}}),\, P_{\text{TX mode}}\right), \\ A_{\text{electronics,tot}}(A_{\text{payload}}) &= 1.96 + 0.49 + A_{\text{payload}} \quad (\text{cm}^2). \end{aligned}$$

In this baseline, the peak shifts from transmission to payload mode only if $P_{\text{payload}} > 95.7 - 40 = 55.7$ mW; otherwise, transmission remains the driver for the CBE. In the

detailed example of Section 4.3, the same substitution $A_{\text{payload}} \rightarrow$ payload area is applied inside the per-block area sum with the appropriate packaging factor κ_{pack} for that block. Figure 2 compiles the baseline footprints and supply powers by function. Blue labels denote the mode-dependent supply power (mW); black labels denote the package area (cm^2). These values are used directly in the mode sums and in $A_{\text{electronics,tot}}$ in Section 3.2.

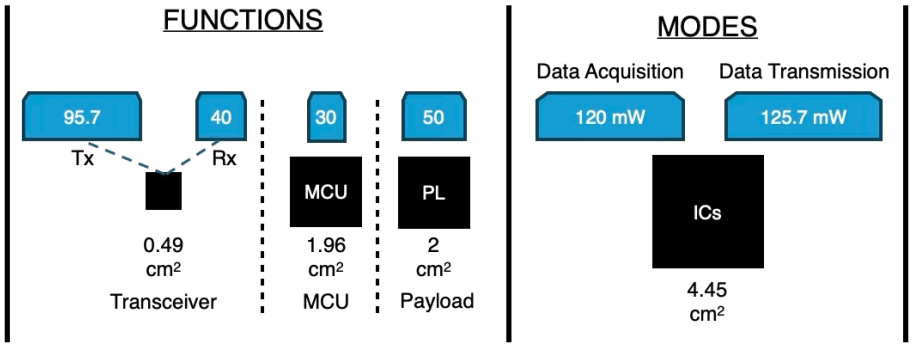

Figure 2. Baseline ICs with footprints (cm^2) and supply powers (mW). Power varies by mode; footprints are fixed. Numbers in blue boxes indicate supply power (mW); numbers in black indicate footprints (cm^2).

Two representative modes are defined: payload (data generation) and transmission (downlink). Active functions by mode are listed in Table 3. Regulators and RF stages beyond the single transceiver are not itemized in this baseline.

Table 3. Representative operational modes and active baseline functions.

Mode	MCU	Payload	Receiver (RX)	Transmitter (TX)
Payload (Data Generation)	ON	ON	ON	OFF
Transmission (Data Downlink)	ON	OFF	OFF	ON

Mode power sums are calculated.
Payload mode:

$$P_{\text{Payload}} = 30 + 50 + 40 = 120 \text{ mW}.$$

Transmission mode:

$$P_{\text{TX}} = 30 + 95.7 = 125.7 \text{ mW}.$$

Peak power (CBE) by using Equation (3):

$$\text{CBE} = \max\left(P_{\text{Payload}}, P_{\text{TX}}\right) = 125.7 \text{ mW}.$$

Contingency and MEV: For CoDR, Class I, a 105% reserve is applied (Table 2) using Equation (4):

$$\text{MEV} = 2.05 \times 125.7 \text{ mW} = 257.7 \text{ mW}.$$

Solar-cell area at normal incidence: Using AM0 $I_{\text{Solar,E}} = 136.1 \text{ mW/cm}^2$ and $\eta_{\text{cell}} = 0.30$ in Equation (5),

$$A_{\text{cell,tot}} = \frac{257.7}{136.1 \times 0.30} = 6.31 \text{ cm}^2.$$

Physical installed cell area (fill ratio): applying Equation (7) with $\eta_{\text{infill}} = 0.94$,

$$A_{\text{cell,phys}} = \frac{6.31}{0.94} = 6.71 \text{ cm}^2.$$

Electronics placement and minimum installed area: The sum of baseline package footprints is $A_{\text{electronics,tot}} = 1.96 + 2.00 + 0.49 = 4.45\ \text{cm}^2$. The end-to-end sizing flow—from mode powers to CBE and MEV, and then to the required solar-cell area at normal incidence—is summarized in Figure 3. For the separated architecture, the recommended minimum installed area is

$$A_{\text{satellite}} = \max\left(A_{\text{cell,phys}},\ A_{\text{electronics,tot}}\right) = \max(6.71,\ 4.45) = 6.71\ \text{cm}^2.$$

Other layouts (half-mixed, mixed/balanced, fully conservative) modify only this final allocation step; see Section 4.1. The more complete, higher-power case with explicit PA/LNA and conversion losses is treated in Section 4.3.

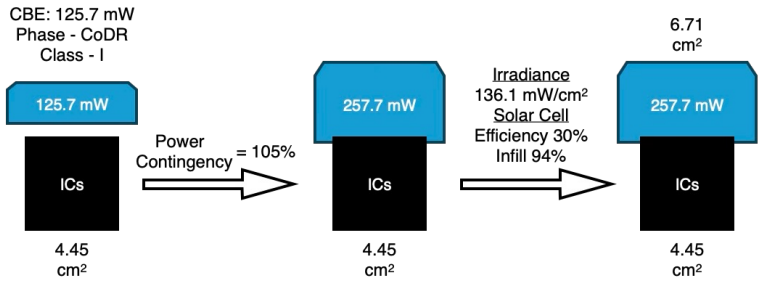

Figure 3. Workflow for sizing the solar array: from mode powers to the CBE (**left**), applying a 105% power contingency to obtain the MEV (**middle**), and computing the required solar-cell area at normal incidence (**right**). Blue boxes denote the solar-cell physical area with the required generated power indicated inside; black boxes denote the ICs footprint. The sizing uses an irradiance of 136.1 mW cm^{-2}, 30% cell efficiency, and 94% infill to derive $A_{\text{cell,tot}}$ (active area) and $A_{\text{cell,phys}}$ (physical area).

4. Detailed Model

This section develops the detailed model. It reuses the canonical sizing relations of Section 3.1 (Equations (4)–(8)), applies the architecture allocations in Section 4.1, and then instantiates the method on a realistic part set.

4.1. Architectural Implications for Minimum Surface Area

The stepwise sizing introduced earlier applies directly to a separated architecture , where power generation and electronics placement are confined to different faces of the satellite. In practice, PlanarSat layouts may also be half-mixed or fully mixed, where electronics and solar cells share surfaces or are distributed across both faces. These alternatives change only the final allocation step that converts the power-driven cell area and the electronics placement area into the installed satellite area. The implications of these choices for the operational envelope are discussed in Section 5. Figure 4 illustrates the four layouts used in this paper. In all cases, only the sunlit face generates power at a given instant; "installed area" is a capacity over time as attitudes change. The half-mixed layout adds pocket cells on the electronics face to improve time-in-mode during illumination flips; the mixed layout enforces per-face sufficiency (either face alone meets MEV), trading installed area for robustness.

Separated architecture. One face is dedicated to solar cells and the other to electronics. The installed area is set by the larger of the physical cell area and the electronics placement area. For the separated layout, the installed area follows (8).

Half-mixed architecture. One face is primarily electronics and the opposite face is primarily solar cells. Any leftover area on the electronics face is also populated with cells. The additional active cell area available on the electronics face is

$$A_{\text{additional,cell}} = \left(A_{\text{satellite}} - A_{\text{electronics,tot}}\right)\eta_{\text{infill}}. \tag{9}$$

These pockets contribute power only when the electronics face is sunlit. Instantaneous generation is never summed across faces. The half-mixed layout is used when electronics placement dominates the installed area; moreover, small residual pockets can be populated with cells to improve time-in-mode statistics under favorable illumination, without changing the MEV target or assuming that these pockets meet any operational mode by themselves. In the presence of a battery or albedo, these smaller cells can provide extra operational time and energy.

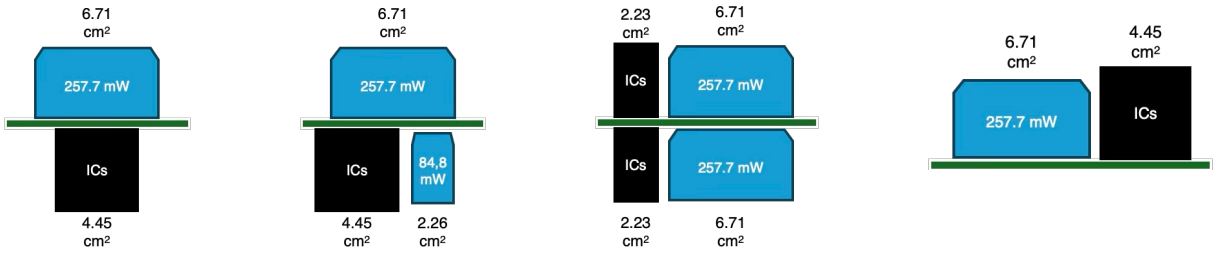

Figure 4. Architectural scenarios for the baseline PlanarSat example: (**a**) separated, (**b**) half-mixed, (**c**) mixed with per-face power sufficiency, and (**d**) fully conservative with all electronics on one side. Instantaneous electrical power is produced by the sunlit face only. "Total installed area" refers to capacity over time as attitudes change, not to simultaneous illumination. In the half-mixed case (**b**), the "pocket" cells on the electronics face contribute power only when that face is sunlit; they are motivated by illumination flips or long intervals with the electronics face being exposed, which increases usable time-in-mode even if these pockets alone cannot support the transmit mode. In the mixed case (**c**), the reported "best-case minimum" assumes per-face power sufficiency, and either face alone meets the MEV when sunlit, trading extra installed area for robustness to which face is illuminated.

Mixed architecture. Both faces host a combination of electronics and solar cells. For a best-case minimum with explicit per-face power sufficiency, either face can meet the MEV when sunlit. This per-face sufficiency provides continuity in the absence of attitude control because it cannot be guaranteed which face is illuminated in orbit. The installed area is bounded by

$$A_{\text{satellite,mixed}} = A_{\text{cell,phys}} + \frac{A_{\text{electronics,tot}}}{2}. \tag{10}$$

which assumes that electronics are split evenly across the two faces. A fully conservative bound, where all electronics end up on one face, is

$$A_{\text{satellite,max}} = A_{\text{cell,phys}} + A_{\text{electronics,tot}}. \tag{11}$$

Equations (10) and (11) are conditioned on per-face sufficiency; relaxing this constraint can reduce the installed area at the cost of the robustness of the face that is sunlit.

Instantiated values for the detailed example.: Using the values derived in Section 4.3, namely $A_{\text{cell,phys}} = 21.47\ \text{cm}^2$ and $A_{\text{electronics,tot}} = 15.72\ \text{cm}^2$, the corresponding installed areas are

$$A_{\text{satellite,min}}\ (\text{separated}) = \max(21.47, 15.72) = 21.47\ \text{cm}^2, \tag{12}$$

$$A_{\text{satellite,mixed}}\ (\text{best case}) = 21.47 + \frac{15.72}{2} = 29.33\ \text{cm}^2, \tag{13}$$

$$A_{\text{satellite,max}}\ (\text{conservative}) = 21.47 + 15.72 = 37.19\ \text{cm}^2. \tag{14}$$

Realistic designs are expected to fall between these analytical bounds, depending on placement, routing, packaging, and mission-specific constraints.

4.2. Method (Detailed Case)

The detailed case reuses the core sizing relations defined in Section 3.1 (Equations (4)–(8)). Mode sums in Section 4.3 already include conversion losses (MPPT and regulation), so no additional division by power-path efficiency is applied when translating the MEV to the solar-cell area. The architecture-dependent allocation remains as in Section 4.1.

4.3. Detailed Sizing Example

This example applies the framework to a concrete hardware set to make the sizing steps explicit and to show how the installed area depends on the surface architecture. The peak power (CBE), the contingency-corrected requirement (MEV), and the derived solar-cell areas are architecture-independent; the architecture only determines how the required cell area coexists with the electronics placement area on the two faces.

4.3.1. Function Blocks and Placement Area

In early PCB design, detailed layouts are rarely available. To avoid underestimation, each function block is allocated a placement area equal to four times the IC footprint (IC area plus an additional three times the IC area for passives, routing, and clearances) (Section 7.1 of [15]). Figure 5 lists the functions, footprints, and supply powers used here. For IC-based blocks, we use $\kappa_{\text{pack}} = 4$ (IC area + 3× passives/routing). The payload is provided as a complete system and is taken as-is, i.e., $\kappa_{\text{pack}} = 1$. Gray shading denotes the additional area allocated to passives and routing per IC, and the orange tags indicate regulator efficiencies applied inside the mode sums. The resulting placement totals yield $A_{\text{electronics,tot}} = 15.72\ \text{cm}^2$, which is used in the architecture allocations below.

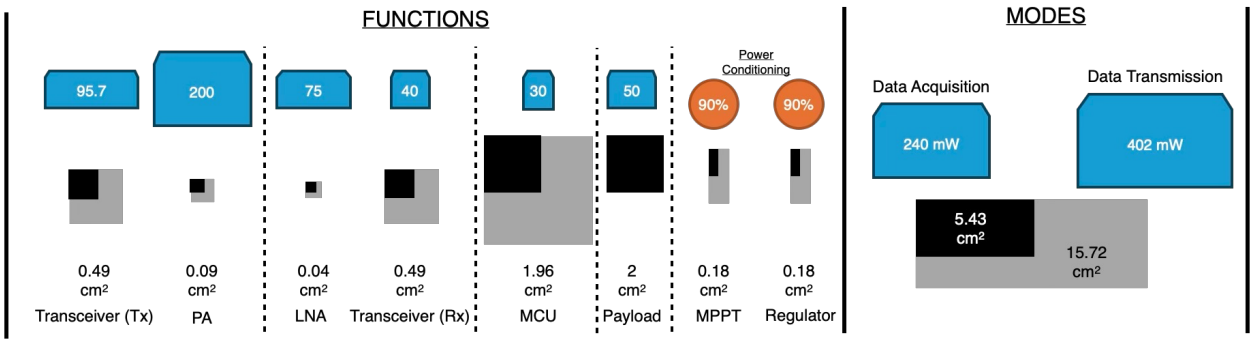

Figure 5. Functions and ICs used in the detailed example. Footprints (cm^2), supply power (mW), estimated peripheral area per IC (gray), and regulator efficiency (orange) are indicated. Unless otherwise noted, each block's total area is four times the IC footprint.

The total electronics placement area is

$$A_{\text{electronics,tot}} = 7.84 + 1.96 + 1.96 + 2.00 + 0.16 + 0.36 + 0.72 + 0.72 = 15.72\ \text{cm}^2.$$

4.3.2. Operational Modes and CBE

Mode power is the sum of active subsystems, scaled by power-path losses (MPPT and regulator assumed 90% each). These conversion losses are included in the mode sums and are not applied again when translating the MEV to solar-cell area via (5)–(7). The representative modes are given in Table 4.

Table 4. Representative operational modes and active subsystems.

Mode	MCU	Payload	Transceiver (RX)	LNA	Transceiver (TX)	PA	MPPT/Reg
Data Acquisition	ON	ON	ON	ON	OFF	OFF	ON
Transmit	ON	OFF	OFF	OFF	ON	ON	ON
Standby	ON	OFF	ON	ON	OFF	OFF	ON

Data acquisition:

$$P_{\mathrm{DA}} = \frac{30 + 50 + 75 + 40}{0.9 \times 0.9} = 240 \text{ mW}.$$

Transmit:

$$P_{\mathrm{TX}} = \frac{30 + 95.7 + 200}{0.9 \times 0.9} = 402 \text{ mW}.$$

Standby:

$$P_{\mathrm{SB}} = \frac{30 + 40 + 75}{0.9 \times 0.9} = 179 \text{ mW}.$$

Peak mode power:

$$\mathrm{CBE} = \max(P_{\mathrm{DA}}, P_{\mathrm{TX}}, P_{\mathrm{SB}}) = 402 \text{ mW}.$$

4.3.3. Power-Path Losses, Contingency, and Solar-Cell Sizing

Power-path losses are modeled with an MPPT and a regulator at 90% efficiency each, consistent with typical values [16,17]. For CoDR, Class I, a 105% contingency is applied (Table 2), using Equation (4):

$$\mathrm{MEV} = 2.05 \times 402 \text{ mW} = 824.1 \text{ mW}.$$

Electrically active cell area at normal incidence: Using Equation (5), $A_{\mathrm{cell,tot}} = \frac{824.1}{136.1 \times 0.30} = 20.18$ cm^2;

Physical area to host the cells (fill ratio $\eta_{\mathrm{infill}} = 0.94$): using Equation (7), $A_{\mathrm{cell,phys}} = \frac{20.18}{0.94} = 21.47$ cm^2. Figure 3 shows the three-step sizing sequence for this baseline: (i) mode powers $\rightarrow$ CBE, (ii) application of the 105% contingency to obtain the MEV, and (iii) translation of the MEV to solar-cell active and physical areas at normal incidence. Blue boxes report the resulting cell area and the required generated power at each step. Figure 6 illustrates the same computation for the detailed case and carries forward the combined electronics placement area so that the layout expressions of Section 4.1 can be applied consistently.

4.3.4. Installed Area by Architecture

Only the sunlit face generates power at any instant. "Installed area" refers to physical area available for cells and electronics on the two faces; it does not imply simultaneous illumination of both faces. Using (7) with the values from 'Power-Path Losses, Contingency, and Solar-Cell Sizing' ($A_{\mathrm{cell,phys}} = 21.47$ cm^2, $A_{\mathrm{electronics,tot}} = 15.72$ cm^2) and the layout expressions in Section 4.1, the installed areas are separated 21.47 cm^2, mixed (per-face sufficiency) 29.33 cm^2, and conservative 37.19 cm^2. Figure 7 shows the corresponding layouts; panels (a)–(c) visualize how the same $A_{\mathrm{cell,phys}}$ and $A_{\mathrm{electronics,tot}}$ map to the installed-area bounds for separated, mixed (per-face sufficiency), and conservative allocations.

For this hardware set, the installed-area ordering is separated < mixed (per-face) < conservative: 21.47 < 29.33 < 37.19 cm^2.

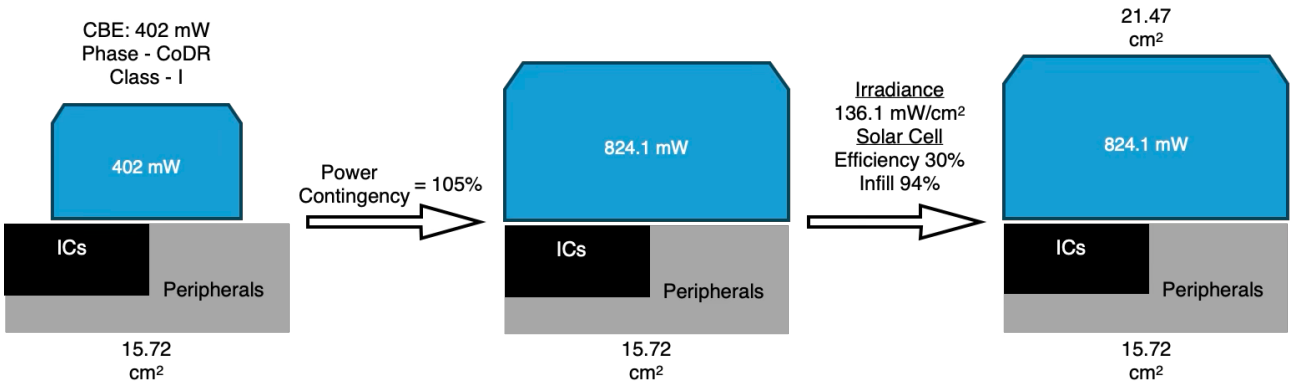

Figure 6. Workflow for sizing the solar array with a realistic electronics footprint. From mode powers to the CBE (**left**), apply a 105% power contingency to obtain the MEV (**middle**); then, compute the required solar-cell area at normal incidence (**right**). Blue boxes denote the solar-cell physical area with the required generated power indicated inside; black boxes denote the ICs; gray boxes denote the area allocated to peripherals and routing required by the ICs. The combined electronics footprint (ICs + peripherals/routing) is 15.72 cm^2 and is carried across the panels. Sizing assumes an irradiance of 136.1 mW cm^{-2}, 30% cell efficiency, and 94% infill to derive $A_{\text{cell,tot}}$ (active area) and $A_{\text{cell,phys}}$ (physical area).

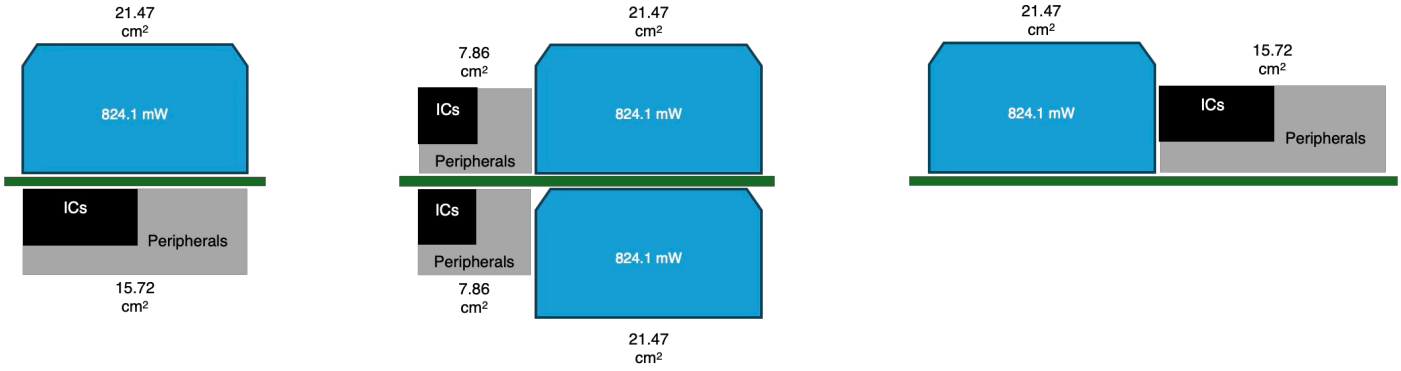

(**a**) Separated (minimum installed area)

(**b**) Mixed, balanced (per-face sufficiency)

(**c**) Conservative (all electronics on one face)

Figure 7. Architecture-dependent installed area for the same hardware set ($A_{\text{cell,phys}} = 21.47$ cm^2, $A_{\text{electronics,tot}} = 15.72$ cm^2). Results: (**a**) $A_{\text{satellite,separated}} = 21.47$ cm^2; (**b**) $A_{\text{satellite,mixed}} = 29.33$ cm^2; (**c**) $A_{\text{satellite,max}} = 37.19$ cm^2.

The separated layout yields the smallest installed area in this example because the power requirement dominates ($A_{\text{cell,phys}} > A_{\text{electronics,tot}}$). The mixed, balanced layout increases the installed area to achieve per-face power sufficiency when either face is sunlit, which improves its robustness to illumination. The conservative case provides a practical upper bound for this hardware set. These architecture choices trade installed areas against margins to illumination and attitude; operational consequences are quantified next via the incidence-angle envelope.

5. Operational Envelope and Design Implications

The operational envelope is the range of Sun–surface incidence angles over which a PlanarSat can sustain its required modes, given its installed area and technology parameters. In what follows, we first derive the geometric envelope from the ratio $\text{CBE}_{\text{mode}}/\text{MEV}$ and then interpret it in the context of the mixed architecture (dual-face) and separated architecture (single-face) layouts used in Figures 8–10. For a given configuration, there exists a maximum incidence angle $\theta_{\max}$ beyond which the available electrical power falls

below the mode demand. Project-phase sizing and contingency shape the envelope: during Bid/CoDR, larger reserves inflate the installed cell area and widen the allowable sun-off-pointing; as designs mature (PDR/CDR) and CBE converges, downsizing arrays save the area at the cost of the envelope margin. This explains why early concepts often show generous angle margins that narrow later.

Assuming a cosine response to incidence, the available electrical power is

$$P_{\text{gen}}(\theta) = P_{\text{gen,max}} \cos\theta. \tag{15}$$

Continuous operation for a mode with demand CBE_{mode} requires

$$\theta_{\text{max}}(\text{mode}) = \arccos\left(\frac{\text{CBE}_{\text{mode}}}{P_{\text{gen,max}}}\right). \tag{16}$$

Consistent with the sizing used throughout the paper, mode sums already include conversion losses, and contingency is applied to obtain MEV. The array is sized at normal incidence to meet MEV, so we take

$$P_{\text{gen,max}} = \text{MEV}. \tag{17}$$

With a fixed contingency policy C, this reduces to

$$\theta_{\text{max}} = \arccos\left(\frac{\text{CBE}}{\text{MEV}}\right) = \arccos\left(\frac{1}{1+C}\right),$$

which ties the envelope directly to the reserve policy (see Appendix A).

Using the detailed example values ($\text{CBE}_{\text{TX}} = 402$ mW, $\text{CBE}_{\text{PL}} = 240$ mW, MEV $= 824.1$ mW), the resulting angles are

$$\theta_{\text{max}}(\text{TX}) = \arccos\left(\frac{402}{824.1}\right) = 60.8^\circ$$

$$\theta_{\text{max}}(\text{Payload}) = \arccos\left(\frac{240}{824.1}\right) = 73.1^\circ.$$

These are the maximum deviations from normal incidence at which the satellite can continuously support transmission and payload modes without energy storage or sun-pointing. Figure 8 aggregates these results. The graph in the middle shows the continuous-operation bands for mixed architectures, $\pm\theta_{\text{max}}$ for modes with the highest CBE, and the transmit from $\theta_{\text{max}} = \arccos(\text{CBE}_{\text{mode}}/\text{MEV})$. The graph on the right represents the separated architecture.

Attitude tendencies in LEO. In free-molecular low Earth orbit, residual drag produces restoring torques that tend to align the largest area broadside to the velocity vector when a nonzero center-of-pressure to center-of-mass offset exists [18–20]. For high area-to-mass designs, such as PlanarSats, this effect can dominate over other perturbations at typical altitudes, promoting passive aerodynamic stabilization [20,21]. This does not fix which face is sunlit at any instant; it influences the statistics of which face is illuminated over time. Throughout this section, we use "broadside to velocity" to represent the drag-maximizing orientation in free-molecular flow, with the panel's surface normal being aligned with the velocity vector.

Orbit-level illustration. To place these envelopes in context, we propagated a two-day orbit at a 0.5 s step in MATLAB R2025a (MathWorks, Natick, MA, USA) using the `satelliteScenario` function with a two-body Keplerian propagator. The initial state was set from the epoch osculating elements consistent with the NinjaSat TLE shown

below [22,23], associated with SpaceX Transporter-9 [24]. Sun vectors were obtained from `planetEphemeris`, and eclipses were detected with a cylindrical-umbra check.

```
1 58341U 23174CP  23332.66373576  .00016972  00000-0  89307-3 0  9999
2 58341  97.4799  45.3459 0010400 177.2905 182.8386 15.15663121  3161
```

Figures 9 and 10 show Sun-incidence angles and time-in-mode results for mixed (dual-face cells) and separated (single-face cells) layouts under otherwise identical assumptions. In Figure 9, the top panel plots the instantaneous Sun–surface incidence on the $+Z$ and $-Z$ faces; dashed lines indicate the transmit (60.8°) and payload (73.1°) thresholds. The middle panel classifies the resulting operational state (eclipse, insufficient power, payload-only, or transmission), and the bottom panel reports the time fractions over the two-day span.

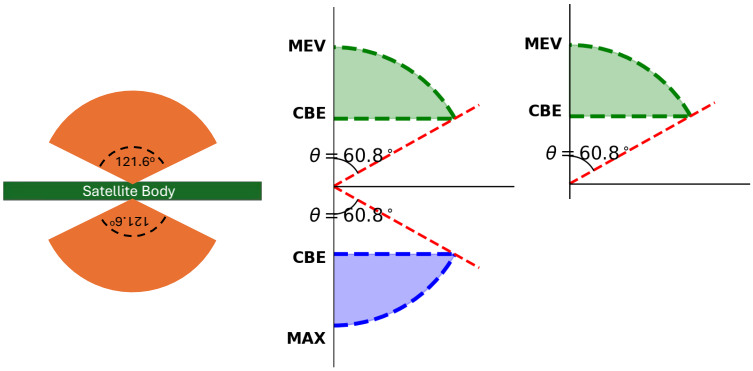

Figure 8. Operational envelope for continuous operation under the detailed example sizing. (**Left**): physical sketch for a mixed, dual-face layout. (**Middle**): angular envelope ($\pm\theta_{\max}$) for transmission and payload modes. (**Right**): single-face case for comparison.

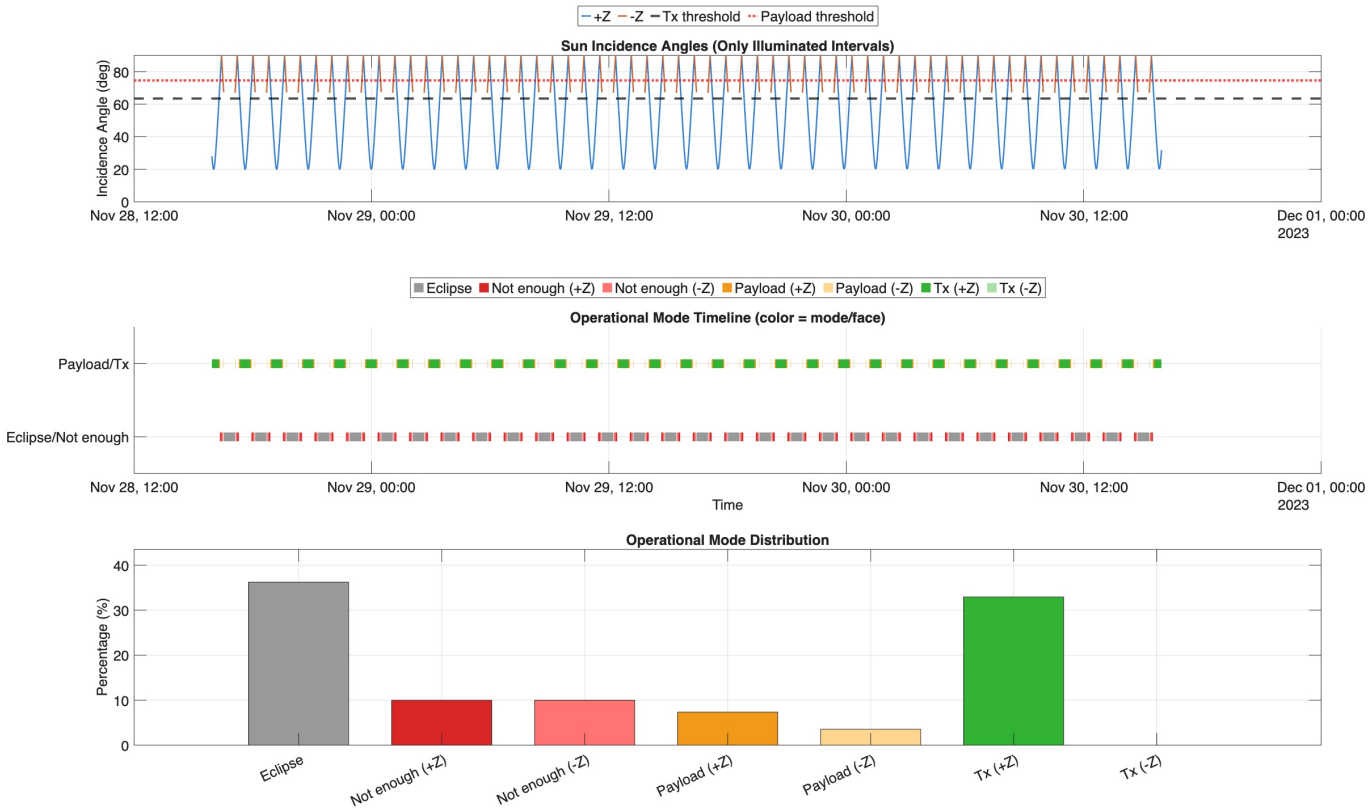

Figure 9. Dual-face cells (mixed, balanced) case. (**Top**): Sun incidence on $+Z$ and $-Z$ faces; dashed thresholds at 60.8° (transmit) and 73.1° (payload). (**Middle**): operational state over time (eclipse, insufficient power, payload-only, transmission). (**Bottom**): fraction of time in each state.

In this propagation, the dual-face case spends approximately 35% of its time in eclipse, 35% in transmission, 12% in payload-only, and 20% with insufficient power, consistent with Figure 9.

Under otherwise identical assumptions, the single-face layout reduces the total operational time by about 15% relative to the dual-face case, as shown in Figure 10. Figure 10 uses the same angle thresholds as Figure 9. Because only one face carries cells, attitude flips that expose the electronics face produce additional "insufficient power" intervals that do not appear in the mixed case, reducing usable time in transmit and payload modes.

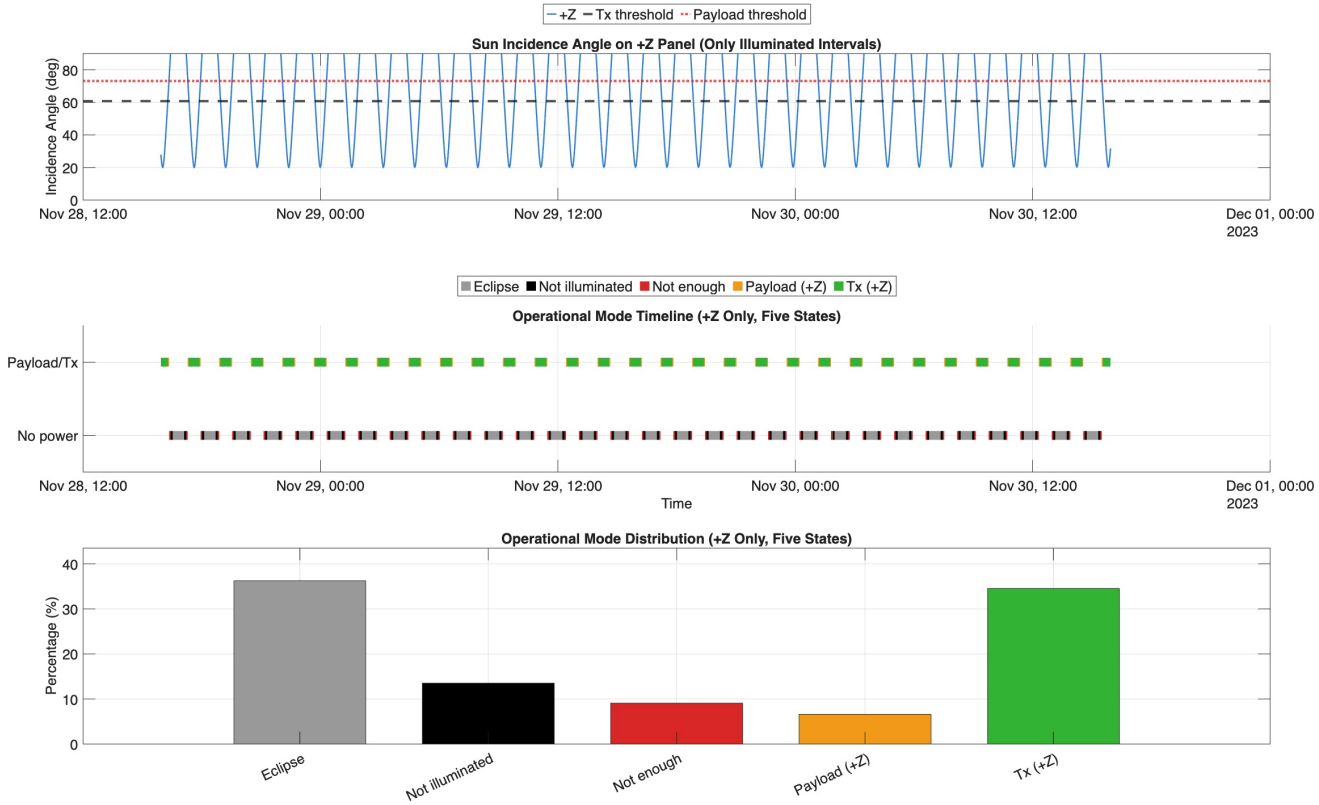

Figure 10. Single-face cells' (separated) case under the same orbit and load assumptions. Compared to the dual-face layout, available time in power-hungry modes is lower and sensitivity to attitude flips is higher.

Design implications. Early design phases typically carry larger contingency, which increases installed cell area and widens the allowable Sun-off-pointing angles. As designs mature and CBE converges, teams may reduce the installed area to save the surface budget at the cost of the envelope margin. Layout also matters. Dual-face layouts that meet the MEV on either face when sunlit improve the statistics of usable illumination, while a single-face layout minimizes the installed area but is more vulnerable to flips and long off-pointing intervals. The specific time-in-mode fractions depend on epoch and orbit geometry and are shown here as representative outcomes.

6. Sensitivity Analysis

We quantify how the required solar-cell area and the continuous-operation angle respond to three parameters while keeping the sizing framework consistent with the rest of the paper: (i) solar-cell efficiency η_{cell}, (ii) power-path efficiency $\eta_{\text{power}} = \eta_{\text{MPPT}}\eta_{\text{reg}}$, and (iii) installed fill ratio η_{infill} [17,25]. Nominal values follow the detailed example: $\eta_{\text{cell}} = 0.30$, $\eta_{\text{power}} = 0.81$, $\eta_{\text{infill}} = 0.94$, $I_{\text{Solar,E}} = 136.1\ \text{mW cm}^{-2}$, $\text{CBE}_{\text{TX}} = 402\ \text{mW}$, and $\text{MEV} = 824.1\ \text{mW}$ (CoDR Class I, 105%). Active and physical cell areas follow

Equations (5)–(7); the continuous-operation angle follows Equation (16) with $P_{\text{gen,max}} = \text{MEV}$ per Equation (17). Each sweep varies one parameter while holding the others fixed. When η_{power} is swept, the mode budgets (CBE and MEV) are recomputed from fixed load powers at fixed contingency CBE/MEV and hence θ_{max} remain unchanged.

Interpretation of Table 5. Changes in η_{cell} and η_{infill} rescale the area but do not alter envelope angles; for the baseline, these remain 60.8° (transmit) and 73.1° (payload). The power-path block shows the area decreasing approximately with $1/\eta_{\text{power}}$ when the CBE or MEV is recomputed from fixed loads, with θ_{max} being constant because CBE/MEV is unchanged. Numerically, improving η_{cell} from 10% to 45% reduces $A_{\text{cell,phys}}$ from 64.4 cm^2 to 14.3 cm^2; improving η_{power} from 0.60 to 0.95 lowers $A_{\text{cell,phys}}$ from 29.0 cm^2 to 18.3 cm^2 (about 37%); raising η_{infill} from 0.85 to 0.95 reduces $A_{\text{cell,phys}}$ from 23.75 cm^2 to 21.25 cm^2 (approximately 10%).

Scope of κ_{pack}. The electronics packing factor κ_{pack} is not swept because it does not enter Equations (5)–(7) or the angles used here. It linearly rescales the electronics placement area via Equation (1), which then maps to the installed area through the architecture rules in Section 4.1. In separated/half-mixed layouts, this influence appears once $A_{\text{electronics,tot}} > A_{\text{cell,phys}}$ (cf. Equation (8)); in mixed layouts, it enters additively (Equations (10) and (11)). Thus, κ_{pack} shifts architecture-dependent installed-area totals (see Figure 7) without changing the sensitivity trends or θ_{max} reported here (Figure 11).

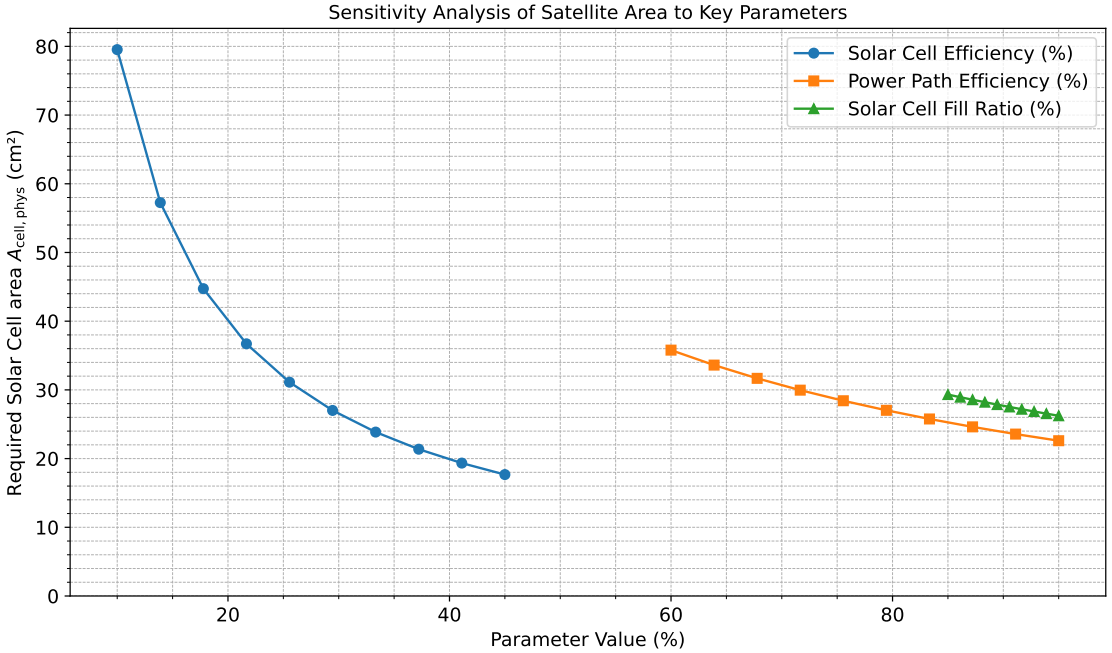

Figure 11. Sensitivity of physical cell area $A_{\text{cell,phys}}$ to η_{cell}, η_{power}, and η_{infill}. Curves illustrate the inverse dependence on multiplicative efficiencies. Note: The curves are computed from $A_{\text{cell,phys}} = \text{MEV}/(I_{\text{Solar,E}}\eta_{\text{cell}}\eta_{\text{power}}\eta_{\text{infill}})$ with MEV held at 824.1 mW; absolute values in the plot therefore differ slightly from Table 5, which treats MEV as including conversion losses and recomputes CBE/MEV when η_{power} is swept. The table provides calibrated values; the plot shows trends. Translation from the cell area to the installed area is architecture-dependent (Section 4.1).

Table 5. Sensitivity of required cell area and envelope angles. CBE and MEV include conversion losses; $I_{\mathrm{Solar,E}} = 136.1\ \mathrm{mW\,cm^{-2}}$. Unless noted, $\eta_{\mathrm{cell}} = 0.30$ and $\eta_{\mathrm{infill}} = 0.94$. For the η_{power} block, the CBE and MEV are recomputed from fixed loads at each η_{power}, so θ_{max} (transmit) remains 60.8° because CBE/MEV is unchanged. Bold values indicate the nominal baseline cases used for comparison in each parameter block.

Parameter	Value	$A_{\mathrm{cell,tot}}$ ($\mathrm{cm^2}$)	$A_{\mathrm{cell,phys}}$ ($\mathrm{cm^2}$)	θ_{max} (TX, deg)
Solar-cell efficiency η_{cell} (with the MEV being fixed at 824.1 mW)				
10%	0.10	60.55	64.42	60.8
20%	0.20	30.28	32.21	60.8
30% (Nom.)	0.30	**20.18**	**21.47**	**60.8**
45%	0.45	13.46	14.31	60.8
Power-path efficiency η_{power} (with the CBE and MEV being recomputed)				
60%	0.60	27.25	28.99	60.8
70%	0.70	23.36	24.85	60.8
81% (Nom.)	0.81	**20.18**	**21.47**	**60.8**
95%	0.95	17.21	18.31	60.8
Fill ratio η_{infill} (with the MEV being fixed at 824.1 mW; $A_{\mathrm{cell,tot}}$ is constant)				
85%	0.85	20.18	23.75	60.8
90%	0.90	20.18	22.43	60.8
94% (Nom.)	0.94	**20.18**	**21.47**	**60.8**
95%	0.95	20.18	21.25	60.8

7. Discussion and Conclusions

This paper presents an analytical framework that links contingency-corrected power demand, solar-array sizing, and electronics placement to estimate the minimum installed surface area of planar, highly miniaturized satellites. In the atto- and femto-class, the surface area often becomes the governing limitation within the stated scope because the same faces must both generate power and host the electronics required for basic functionality.

Methodologically, the framework provides closed-form expressions that connect contingency policy and peak-mode demand to required active and physical cell areas, convert these into architecture-dependent installed-area bounds, and then map the resulting capacity to a geometric operational envelope and orbit-level time-in-mode statistics. These results are intended for early-phase feasibility; detailed thermal, link-budget, and structural trades are orthogonal and planned for future work.

First, the minimum installed area for a separated layout is set by whichever requirement is larger: the physical solar-cell area needed to meet the contingency-corrected peak load at normal incidence, or the total electronics placement area. This separates the problem into an architecture-independent sizing of power and a layout-dependent allocation on the faces.

Second, architecture changes only the allocation step. Separated layouts minimize the installed area when power dominates; mixed layouts increase the installed area if per-face power sufficiency is desired, which improves the robustness to which face is sunlit; and placing all electronics on one face provides a conservative upper bound. These bounds are quantified in Section 4.1 and illustrated in Figure 7 for the detailed example.

Third, the operational envelope follows directly from the ratio of the contingency-corrected power capacity to the mode demand under a cosine law. With the mode sums already accounting for conversion losses and with contingency applied once, the resulting continuous-operation angles reported in Section 5 map installed area and technology choices to time-in-mode capability without introducing additional loss factors.

Fourth, the sensitivity study in Section 6 shows distinct roles for the technology parameters. A higher solar-cell efficiency and a higher fill ratio primarily reduce the area required to meet the contingency-corrected load at normal incidence. Improvements in

power-path efficiency reduce the inflated mode sums and therefore reduce the required area; for a fixed contingency policy, they do not alter the envelope angle derived from the ratio of demand to contingency-corrected capacity. These observations identify where technology development most effectively enables further miniaturization.

Contingency selection directly trades the installed area against the operational margin and should reflect the project phase and risk class (Table 2). Architectures should be chosen with explicit acknowledgment of illumination statistics: separated layouts minimize areas; balanced mixed layouts provide per-face sufficiency when sunlit and are less sensitive to attitude flips. The framework supports rapid feasibility checks by keeping the power sizing architecture-independent and then applying layout expressions to obtain the installed area and the resulting envelope.

The analysis treats continuous operation without energy storage and focuses on power generation and planar integration. Attitude behavior is represented through Sun-incidence geometry rather than closed-loop control. Thermal management, radiation tolerance, electromagnetic compatibility, antennas and link budgets, deployables, and detailed structural effects are not sized here. Within these boundaries, the results provide a lower bound on the installed area for the stated function set.

The same expressions can be re-evaluated as technology parameters, with contingencies evolving across design phases. Natural extensions include coupling the power sizing to duty-cycled operations and batteries, integrating thermal and link-budget constraints, and examining multi-phase design evolutions that show how early contingency and architecture choices propagate to time-in-mode performance in representative orbits.

Author Contributions: Conceptualization, M.Ş.U.; methodology, M.Ş.U.; software, M.Ş.U.; validation, M.Ş.U.; formal analysis, M.Ş.U.; investigation, M.Ş.U.; resources, M.Ş.U.; data curation, M.Ş.U.; writing—original draft preparation, M.Ş.U.; writing—review and editing, M.Ş.U. and A.R.A.; visualization, M.Ş.U.; supervision, A.R.A.; project administration, M.Ş.U.; funding acquisition, M.Ş.U. and A.R.A. All authors have read and agreed to the published version of the manuscript.

Funding: This research received no external funding.

Institutional Review Board Statement: Not applicable.

Informed Consent Statement: Not applicable.

Data Availability Statement: The original contributions presented in the study are included in the article; further inquiries can be directed to the corresponding author.

Acknowledgments: The authors thank Onur Çelik, Stefano Speretta and Erdem Turan for their feedback, comments and support.

Conflicts of Interest: The authors declare no conflicts of interest.

Abbreviations

The following abbreviations are used in this manuscript:

AIAA	American Institute of Aeronautics and Astronautics
AM0	Air Mass Zero (extraterrestrial solar spectrum)
Bid	bidding
BOL	beginning of life (solar-cell rating)
CBE	current best estimate
CDR	critical design review
CoDR	concept design review
COMM	communication
CoM	center of mass

CoP	center of pressure
EOL	end of life (solar-cell rating)
FRR	flight readiness review
IC	integrated circuit
LEO	low Earth orbit
LNA	low-noise amplifier
MCU	microcontroller
MEV	maximum expected value
MPPT	maximum power point tracking
OBC	on-board computer
PA	power amplifier
PCB	printed circuit board
PDR	preliminary design review
PRR	production readiness review
RF	radio frequency
RX	receiver (mode)
TLE	two-line element
TX	transmitter (mode)

Appendix A. Operational Envelope: Derivation and Alternatives

Appendix A.1. Baseline Derivation (Used in the Paper)

We size the array at normal incidence to meet the contingency-corrected peak load, $\mathrm{MEV} = (1 + C)\,\mathrm{CBE}$. Taking $P_{\mathrm{gen,max}} = \mathrm{MEV}$ and a cosine law,

$$\theta_{\max}(\mathrm{mode}) = \arccos\left(\frac{\mathrm{CBE}_{\mathrm{mode}}}{P_{\mathrm{gen,max}}}\right) = \arccos\left(\frac{\mathrm{CBE}_{\mathrm{mode}}}{\mathrm{MEV}}\right).$$

If the peak mode sets $\mathrm{CBE} = \max_{\mathrm{mode}} \mathrm{CBE}_{\mathrm{mode}}$, then $\theta_{\max} = \arccos\big(1/(1 + C)\big)$ for that peak mode. Thus, the envelope reflects the chosen contingency policy by design; it is not an error.

Appendix A.2. Alternative A (Capacity-Margin Form)

Let $M_{\mathrm{mode}} = P_{\mathrm{gen,max}}/\mathrm{CBE}_{\mathrm{mode}}$ be the installed capacity margin for the mode. Then, $\theta_{\max} = \arccos(1/M_{\mathrm{mode}})$. If the team oversizes (or derates to EOL) such that $P_{\mathrm{gen,max}} \neq \mathrm{MEV}$, the envelope depends on M_{mode} rather than directly on C.

Appendix A.3. Alternative B (Orbit/Incidence Derating)

If orbit statistics are folded into sizing via $\gamma_{\mathrm{orbit}} \in (0, 1]$, then $A_{\mathrm{cell,tot}} = \mathrm{MEV}/(I_0\,\eta_{\mathrm{cell}}\,\gamma_{\mathrm{orbit}})$ and $P_{\mathrm{gen,max}} = \mathrm{MEV}$ remains the sizing target, while the usable average margin is effectively reduced by γ_{orbit}. Teams can either (i) keep $\gamma_{\mathrm{orbit}} = 1$ and interpret Figure 8 as a geometric check (our choice here), or (ii) pick $\gamma_{\mathrm{orbit}} < 1$ and treat the figure as a conservative, derated envelope. Avoid double counting.

Appendix A.4. How to Read Figure 8

Dashed angles mark $\theta_{\max}$ per mode; operation is continuous when the instantaneous Sun–surface incidence stays within the corresponding band while sunlit (eclipse intervals bring generation to zero). Changing C widens/narrows these bands; oversizing or end of life (EOL) derating changes M and, thus, the angles under Alternative A.

References

1. Uludağ, M.Ş.; Aslan, A.R. Highly-miniaturized spacecraft "PlanarSat": Evaluating prospects and challenges through a survey of femto & atto satellite missions. *Acta Astronaut.* **2025**, *236*, 343–358. [CrossRef]

2. Johnstone, A. CubeSat Design Specification. 2022. Available online: https://static1.squarespace.com/static/5418c831e4b0fa4ecac1bacd/t/62193b7fc9e72e0053f00910/1645820809779/CDS+REV14_1+2022-02-09.pdf (accessed on 6 June 2025).
3. Radu, S.; Uludag, M.; Speretta, S.; Bouwmeester, J.; Dunn, A.; Walkinshaw, T.; Cas, P.K.D.; Cappelletti, C. The PocketQube Standard. 2018. Available online: https://static1.squarespace.com/static/53d7dcdce4b07a1cdbbc08a4/t/5b34c395352f5303fcec6f45/1530184648111/PocketQube+Standard+issue+1+-+Published.pdf (accessed on 13 June 2025).
4. Franzese, V. PocketQube picosatellites: Survey of missions and technologies. *CEAS Space J.* **2025**. [CrossRef]
5. Bouwmeester, J.; Guo, J. Survey of worldwide pico- and nanosatellite missions, distributions and subsystem technology. *Acta Astronaut.* **2010**, *67*, 854–862. [CrossRef]
6. Barnhart, D.J.; Vladimirova, T.; Baker, A.M.; Sweeting, M.N. A low-cost femtosatellite to enable distributed space missions. *Acta Astronaut.* **2009**, *64*, 1123–1143. [CrossRef]
7. Barnhart, D.J.; Vladimirova, T.; Sweeting, M.N. Very-Small-Satellite Design for Distributed Space Missions. *J. Spacecr. Rocket.* **2007**, *44*, 1294–1306. [CrossRef]
8. Niccolai, L.; Bassetto, M.; Quarta, A.A.; Mengali, G. A review of Smart Dust architecture, dynamics, and mission applications. *Prog. Aerosp. Sci.* **2019**, *106*, 1–14. [CrossRef]
9. STMicroelectronics. *STM32L496RG—Ultra-Low-Power with FPU Arm Cortex-M4 MCU 80 MHz with 1 Mbyte Flash, USB OTG, LCD, DFSDM*; STMicroelectronics: Geneva, Switzerland, 2024. Available online: https://www.st.com/en/microcontrollers-microprocessors/stm32l496rg.html (accessed on 24 May 2025).
10. Azur Space. *3G30A Triple-Junction Solar Cell Assembly Datasheet*; Azur Space: Heilbronn, Germany, 2025. Available online: https://www.azurspace.com/images/products/0003401-01-01_DB_3G30A.pdf (accessed on 25 May 2025).
11. Uludağ, M.Ş.; Aslan, A.R. Power Contingency/Margin Methodology and Operational Envelope Analysis for PlanarSats. *Aerospace* **2025**, *12*, 858. [CrossRef]
12. American Institute of Aeronautics and Astronautics. Guide for Estimating and Budgeting Weight and Power Contingencies for Spacecraft Systems. 1992. Available online: https://webstore.ansi.org/preview-pages/AIAA/preview_G-020-1992.pdf (accessed on 25 May 2025).
13. Brown, C.D. *Elements of Spacecraft Design*; American Institute of Aeronautics and Astronautics, Inc.: Reston, VA, USA, 2002. [CrossRef]
14. Semtech Corporation. *SX1278—137MHz to 525MHz Low Power Long Range Transceiver*; Semtech Corporation: Camarillo, CA, USA, 2024. Available online: https://www.semtech.com/products/wireless-rf/lora-connect/sx1278 (accessed on 24 May 2025).
15. Johnson, H.W.; Graham, M. *High-Speed Digital Design: A Handbook of Black Magic*; Prentice Hall PTR: Upper Saddle River, NJ, USA, 2003.
16. STMicroelectronics. *SPV1040—High-Efficiency Solar Battery Charger with Embedded MPPT*; STMicroelectronics: Geneva, Switzerland, 2021. Available online: https://www.st.com/en/power-management/spv1040.html (accessed on 27 May 2025).
17. Ravindran, R.; Massoud, A.M. State-of-the-Art DC-DC Converters for Satellite Applications: A Comprehensive Review. *Aerospace* **2025**, *12*, 97. [CrossRef]
18. NASA-National Aeronautics and Space Administration. Space Vehicle Design Criteria/Guidance and Control. Technical Report, NASA. 1971. Available online: https://ntrs.nasa.gov/api/citations/19710016459/downloads/19710016459.pdf (accessed on 25 May 2025).
19. Wertz, J.R.; Everett, D.F.; Puschell, J.J. (Eds.) *Space Mission Engineering: The New SMAD*; Microcosm Press: Hawthorne, CA, USA, 2011.
20. Rawashdeh, S.A.; Lumpp, J.E. Aerodynamic Stability for CubeSats at ISS Orbit. *J. Small Satell.* **2013**, *2*, 85–104.
21. Umansky-Castro, J.S.; Yap, K.G.; Peck, M.A. ChipSats for Planetary Exploration: Dynamics and Aerothermal Modeling of Atmospheric Entry and Dispersion. *Front. Astron. Space Sci.* **2021**, *8*, 664215. [CrossRef]
22. Tamagawa, T.; Enoto, T.; Kitaguchi, T.; Iwakiri, W.; Kato, Y.; Numazawa, M.; Mihara, T.; Takeda, T.; Ota, N.; Watanabe, S.; et al. NinjaSat: Astronomical X-ray CubeSat observatory. *Publ. Astron. Soc. Jpn.* **2025**, *77*, 466–479. [CrossRef]
23. Space-Track.org. Space–Track. 2025. Available online: https://www.space-track.org/ (accessed on 25 June 2025).
24. Exolaunch. Mission 24. 2024. Available online: https://www.exolaunch.com/mission_24 (accessed on 25 June 2025).
25. National Renewable Energy Laboratory. Interactive Best Research-Cell Efficiency Chart. 2025. Available online: https://www.nrel.gov/pv/interactive-cell-efficiency.html (accessed on 18 June 2025).